Supporting Information

for

Electrochemically induced Fenton reaction of few-layer MoS_2 nanosheets: Preparation of luminescent quantum dots via a transition of nanoporous morphology

Bang Lin Li,[a] Ling Xiao Chen,[a] Hao Lin Zou,[a] Jing Lei Lei,[b] Hong Qun Luo*[a] and Nian Bing Li*[a]

[a] *Key Laboratory of Eco-environments in Three Gorges Reservoir Region (Ministry of Education), School of Chemistry and Chemical Engineering, SouthwestUniversity, Chongqing 400715, P.R. China. Fax: +86-23-68253237. Tel: +86-23-68253237. E-mail: linb@swu.edu.cn (N. B. Li); luohq@swu.edu.cn (H. Q. Luo).*

[b] *School of Chemistry and Chemical Engineering, Chongqing University, Chongqing 400044, P.R. China.*

1. Electro-generation of H_2O_2 in situ.

It is known that the oxidation of 3,3,5,5-tetramethylbenzidine (TMB) by hydrogen peroxide produces a blue color with major absorption peaks at 370 and 650 nm under acidic condition according to the following equation, which can be recorded in a UV-vis absorption spectrum.[S1]

$$TMB + H_2O_2 \rightarrow oxTMB + H_2O \quad (1)$$

Therefore, the quantitative analysis of oxidation products of TMB can be conducted using UV-vis absorption spectrometry. The signal for oxidation of TMB by H_2O_2 in an absorption spectrum could be used to confirm the generation of H_2O_2 in electrochemical process (Fig. S1A). We can see from Fig. S1A that no obvious absorption signals are observed from TMB solution without any exterior additions (curve a), with saturation of oxygen gas (curve b), and applied with potential of -0.5 V (curve c) after reaction for 10 min, whereas two strong absorption bands peaked at 370 and 650 nm are found in TMB solution when applied with potential of -0.5 V under the condition of saturated oxygen gas (curve d) after reaction for 10 min. It was demonstrated that as the combined action of electrochemical process and the presence of O_2, the pre-Fenton reagent, H_2O_2, was generated. The time-dependent absorbance at 650 nm for TMB solution in the presence of a certain amount of H_2O_2 and being applied by an electrochemical process with saturated O_2 are shown in Fig. S1B. From Fig. S1B, it can be seen that the absorption values at 650 nm continually increase in the TMB solution with the application of

potential of -0.5 V and saturated O_2, whereas with only the initial addition of high concentration of H_2O_2, the increase in absorbance of TMB solution is obviously observed in the beginning but it reaches the highest value after reaction for 2 min. Hence, the results shown in Fig. S1B could be used to demonstrate that the continuous electro-generation of H_2O_2 in situ was induced by electrochemical process in the presence of saturated oxygen.

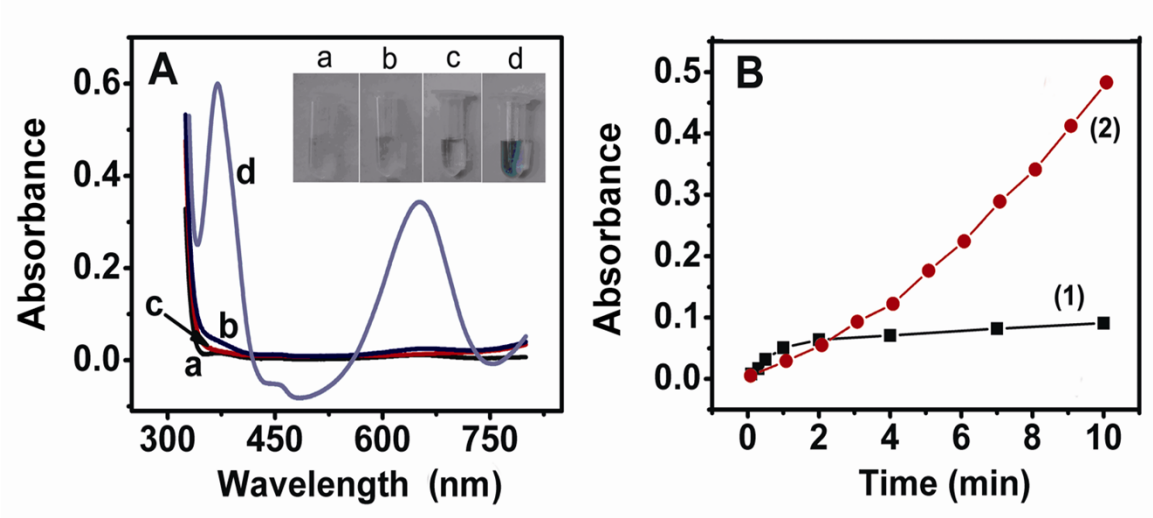

Fig. S1 (A) UV-vis absorption spectra and photographs (insets) of TMB (0.5 mM) solutions without the exterior additions (a), with saturation of oxygen gas (b), applied with potential of -0.5 V (c), and applied with potential of -0.5 V under the condition of saturated oxygen gas (d) after reaction for 10 min. (B) The time-dependent UV-vis absorption at 650 nm for 0.5 mM TMB solution in the presence of 5 M H_2O_2 (1) and with applied potential of -0.5 V under the condition of saturated oxygen at atmospheric pressure (2).

2. Exploration to electro-Fenton reaction

Rhodamine B (RhB) is a kind of organic contaminant, which can be degraded in the presence of · OH. Hence, in the environmental treatments, RhB has been used as a model pollutant to explore the process of electro-Fenton oxidation and optimize the conditions of treatment.[S2] The decay of RhB concentration exhibits an exponential behavior indicating a first-order reaction kinetic for its oxidation by · OH

$$RhB + \cdot OH \rightarrow \text{oxidation production} \quad (2)$$

Assuming the steady-state approximation for ·OH in the electro-Fenton process, the RhB oxidation rate expression can be written as follows:

$$-(d[RhB]/d[t]) = k\,[\cdot OH]\,[RhB] = k_{app}[RhB] \quad (3)$$

which can be integrated to give the following expression:

$$\ln([RhB]_0/[RhB]_t) = k_{app}t \quad (4)$$

where $[RhB]_0$ and $[RhB]_t$ are the concentrations of RhB at the beginning and at time t, respectively, while k_{app} (= k[· OH]) is the apparent pseudo-first-order rate constant. In our experiment, the conditions of electro-Fenton process were explored and further optimized using RhB as the substrate. RhB was added before the initiation of the electro-Fenton reaction. Following initiation, the reaction was monitored using spectrophotometry at various times and the results are shown in Fig. S2a. Apparent pseudo-first-order rate constant (k_{app} = 0.00417) for the oxidative degradation of RhB was determined by plotting $\ln([RhB]_0/[RhB]_t)$ against time in our electro-Fenton system, shown in Fig. S2b.

According to Equation 4, the RhB oxidation rate equation was integrated as $\ln(C_0/C_t)$ = 0.00417t. Therefore, it was demonstrated that with the consumption of ·OH in the degradation of RhB, the total amount of· OH in the electro-Fenton system kept almost constant. The controllability of electro-Fenton process was confirmed through conducting the experiment about the degradation of RhB. Meanwhile, when a specific condition for electro-Fenton process was decided, the impact of · OH on the substrate only depended on the time of reaction.

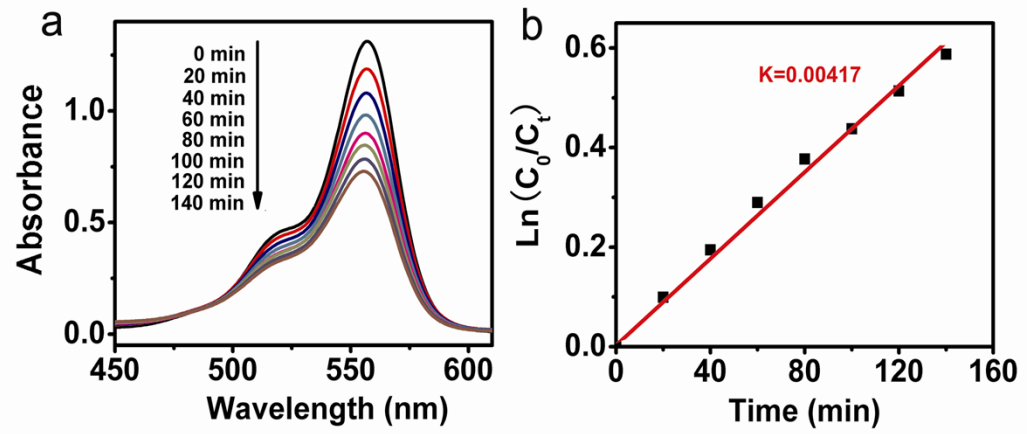

Fig. S2 (a) UV-vis absorption spectra of 0.5 mM RhB aqueous solution applied by electro-Fenton process after reaction for various times. (b) Kinetic analysis for the pseudo-first order reaction between RhB and · OH during electro-Fenton process shown in panel a. Condition: [RhB] = 0.5 mM; V = 50 mL; $[Fe^{2+}]$ = 20 mM; applied potential = -0.5 V; pH = 3.

3. Optimization of electro-Fenton conditions

The conditions of electro-Fenton process were discussed and the oxidation efficiency of Fenton reactions depended on the conditions of electro-Fenton process, such as the value of pH, applied potential, and the initial concentration of Fe^{2+} in the system. Those three factors were explored to obtain the optimal conditions of hydroxyl radicals generation in electro-Fenton system. As shown in Fig. S3a, The optimal pH for the Fenton reaction efficiency is shown to be 3. The hydrogen evolution reaction was induced at more acidic pH values less than 3, resulting in the generation of H_2O_2 in cathodic reaction slow and it further declined the efficiency of electro-Fenton reaction. However, at more basic pH values (>3), the oxidation efficiency of rhodamine B also decreased, which was ascribed to that the iron was converted from a hydrated ferrous form to a colloidal ferric form, thereby causing a decrease in the effectiveness of the reaction. For the optimal Fenton reaction efficiency, the initial pH of $FeSO_4$ solution was adjusted to 3 using sulfuric acid and it remained almost constant over the whole process. This value was selected as the optimum pH to carry out Fenton reaction, according to previous studies on electro-Fenton process.[S3,S4] The optimal value for applied potential in electro-Fenton process was found to be -0.5 V (Fig. S3b). Lower potential (< -0.5 V) was detrimental to the generation of H_2O_2 and applied potentials higher than -0.5 V not only accelerated H_2O_2 reduction to water but also favored the secondary reaction of hydrogen evolution.[S5] It was found that the potential at about -0.5 V under the

oxygenated condition was stronger than that under the deoxygenated one.[S6] Even though the Fe^{2+} can be regenerated in electro-Fenton process, accompanying the electrogeneration of H_2O_2, it was also necessary to explore the effect of initial concentration of Fe^{2+} (Fig. S3c).

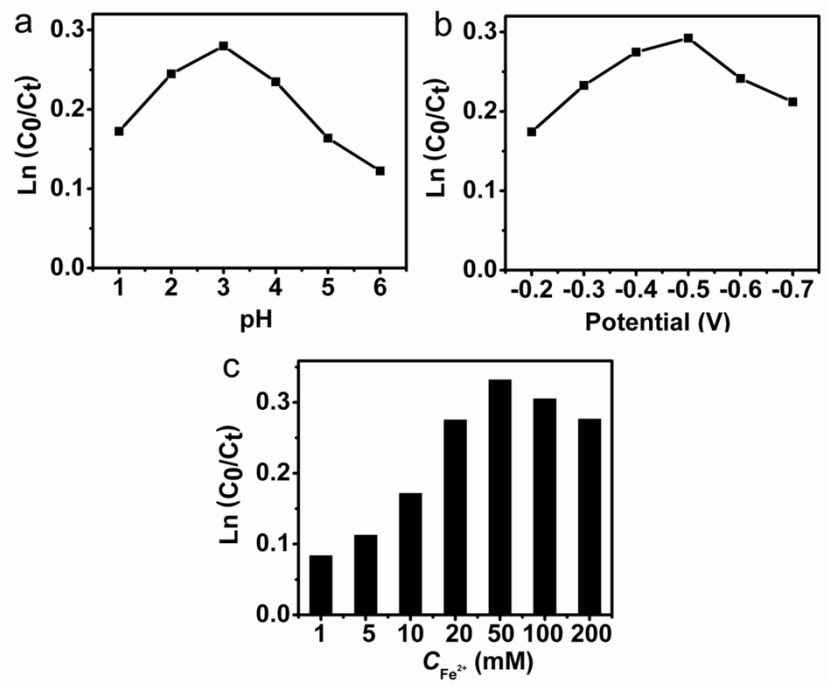

Fig. S3 Optimization of the conditions of electro-Fenton process. (a) Influence of pH in electro-Fenton system on the degradation efficiency of RhB after reaction for 60 min. Operating conditions: applied potential = -0.5 V; [Fe^{2+}] = 20 mM. (b) Influence of applied potential on the degradation efficiency of RhB after reaction for 60 min. Operating conditions: pH = 3; [Fe^{2+}] = 20 mM; (c) Influence of the concentration of Fe^{2+} on the degradation efficiency after reaction for 60 min. Operating conditions: pH = 3; applied potential = -0.5 V. The other conditions for (a), (b), and (c) are the same as in Fig. S1.

4. Electro-Fenton process of graphene oxide monitored by atomic force microscopy

The electro-Fenton reaction of GO was carried out and the morphological change of GO sheets was recorded in AFM. Before the electro-Fenton reaction, the GO sheets deposited on freshly cleaved mica substrate were characterized and the result is shown in Fig. S4a. From Fig. S4a, the bulk sheets possessing the size of about 400 nm and thickness of approximately 1.5 nm (Fig. S4c) were observed. After reaction for 60 min, the products of electro-Fenton reaction were also deposited on freshly cleaved mica substrate and observed in AFM (Fig. S4b). It was obviously observed that the large size of sheets shown in Fig. S4a disappeared, turning into a great deal of small dots (such as section B, D, and E) and a spot of smaller sheets (such as section C). The smaller sheets with the size of below 100 nm and height of 1.5 nm (Fig. S4b, region C) were supposed to be the GO remainders, which were hard to be reacted in electro-Fenton process. Nevertheless, as shown in Fig. S4d, the small dots possessing the height of approximately 0.7 nm were the products of GO sheets in electro-Fenton reaction. The massive hydroxyl radicals generated by electro-Fenton reaction made the GO sheets break into GO dots, further demonstrated to be graphene quantum dots.

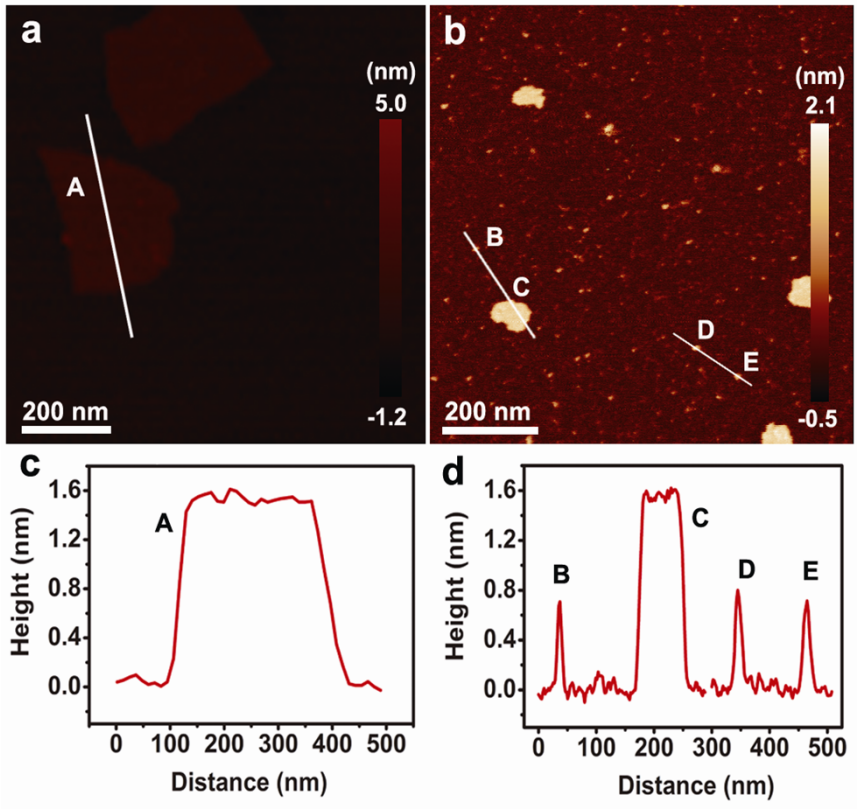

Fig. S4 AFM images of the GO sheets (a) and GO sheets after being treated with electro-Fenton reaction for 60 min (b). (c) Height distribution of a GO sheet. (d) Height distribution of the as-generated dots shown in panel b.

5. UV-vis absorption spectra of GO and as-prepared GQDs

The UV-vis spectra of GO dispersed in water before and after the electro-Fenton reaction were recorded. As shown in Fig. S5, the GO has two UV-vis absorption peaks at 230 and 304 nm, corresponding to π to π* transition of aromatic sp^2 domains and n to π* transition of C=O bond, respectively. Furthermore, two UV-vis absorption peaks centered at 210 and 276 nm are observed after the GO solution reacted with the electro-Fenton reagent, which are similar to those of GQDs prepared from hydrothermal graphene oxide reduction method (230 and 320 nm) and microwave-assisted hydrothermal method (228 and 282 nm).[S7, S8] The origin of these absorptions can be ascribed to π electron transition in oxygen-containing GQDs. The stronger absorption peak at 210 nm corresponds to a good deal of π to π* transition of aromatic sp^2 domains,[S7] and the absorption at 276 nm is due to n to π* transition of C=O bond, located in the edge of GQDs.[S8]

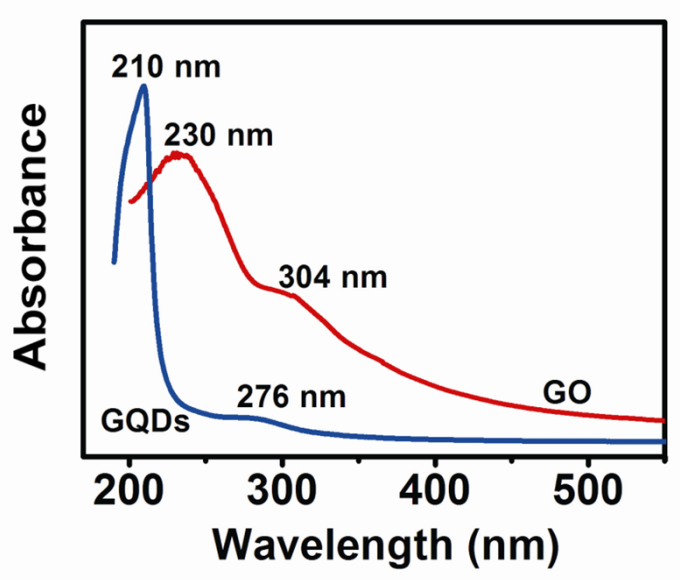

Fig. S5 UV-vis absorption spectra of GO and as-prepared GQDs aqueous solution.

6. Remove of surfactant in exfoliated MoS_2 nanosheets solution.

The high concentration of surfactant in initial MoS_2 nanosheets was considered to be a problem for the subsequent researches. Therefore, before carrying out the following experiments, the purification of MoS_2 nanosheets must be conducted. In the previous report,[S9] the initial MoS_2 nanosheets solution was dropped into a plane to form thin film and then the film was washed with ultrapure water to remove the surfactant. However, this route was time-consuming and lowly efficient. We found that almost all MoS_2 nanosheets can be collected from mixture solution as sediments after centrifuged at 12000 rpm. On the basis of results, the purification of MoS_2 nanosheets from sodium cholate was carried out using centrifugation. The mixture solution was centrifuged at 12000 rpm for 30 min, and sediments were separated and further dispersed in ultrapure water. The regenerated dispersion was centrifuged at 12000 rpm for 30 min, followed by the collection of sediments to complete the washing process. The washing process was repeated for other two times to remove surfactant sodium cholate completely. The thermogravimetric analysis (TGA) data for four samples are shown in Fig. S6. Sodium cholate was oxidized at 320 °C, while the MoS_2 powder began to be oxidized when the temperature was increased to 520 °C (curve b). Meanwhile, MoS_2 nanosheets solid mixture without purification was also oxidized at 320 °C, indicating that vast sodium cholate existed. It is obviously observed that the surfactant peak identified in Fig. S6 (curve a) at about 320 °C has disappeared in MoS_2 nanosheets after purification. This demonstrates that the vast majority of surfactant can be removed by washing and centrifugation treatment.

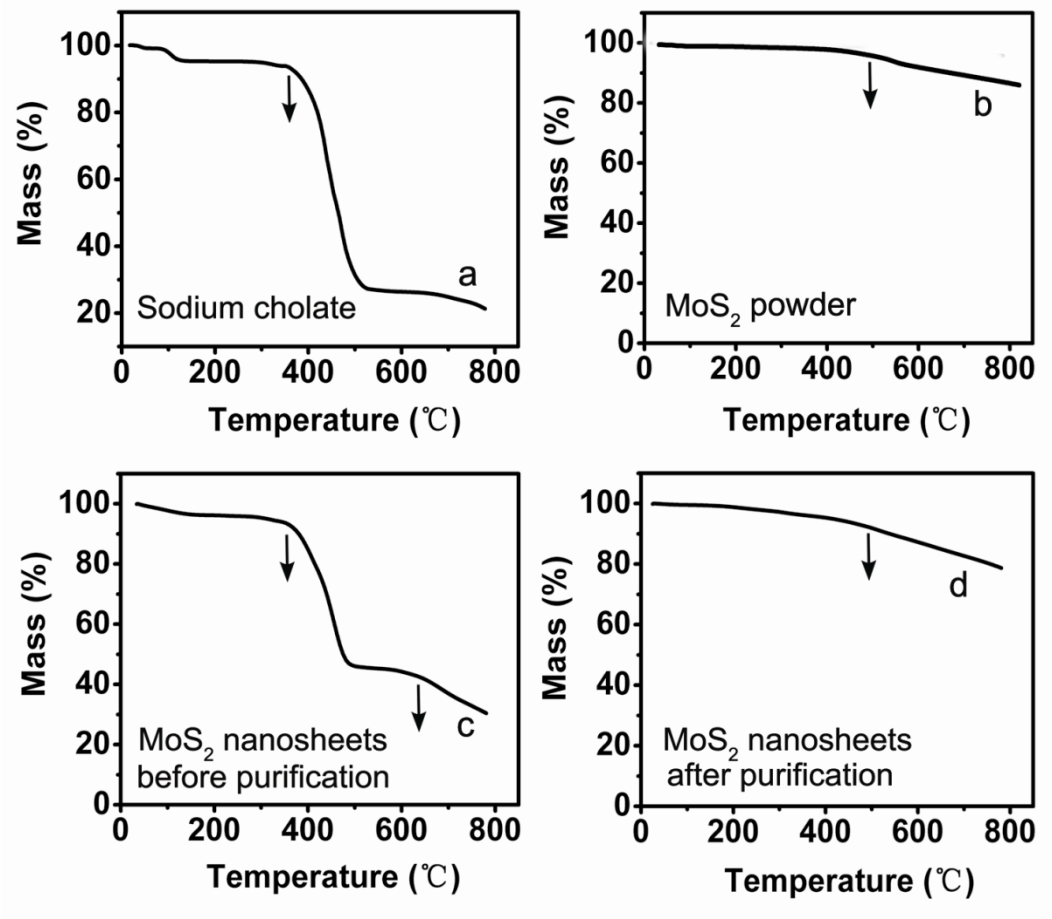

Fig. S6 Thermogravimetric analysis data for sodium cholate (a), MoS_2 powder (b), exfoliated MoS_2 nanosheets before the process of purification (c), and MoS_2 nanosheets after the treatment of purification (d).

References

[S1] Y. Lin, Z. Li, Z. Chen, J. Ren and X. Qu, *Biomaterials*, 2013, **34**, 2600.

[S2] W. Liu, Z. Ai and L. Zhang, *J. Hazard. Mater.*, 2012, **243**, 257.

[S3] E. Brillas, B. Boye, I. Sirés, J. A. Garrido, R. M. Rodríguez, C. Arias, P. L. Cabot and C. Comninellis, *Electrochim. Acta*, 2004,**49**, 4487.

[S4] N. Oturan, M. Zhou and M. A. Oturan, *J. Phys. Chem. A*, 2010, **114**, 10605.

[S5] N. Oturan, M. Panizza and M. A. Oturan, *J. Phys. Chem. A*, 2009, **113**, 10988.

[S6] H. Liu, C. Wang, X. Li, X. Xuan, C. Jiang and H. N. Cui, *Environ. Sci. Technol.*, 2007, **41**, 2937.

[S7] D. Pan, J. Zhang, Z. Li and M. Wu, *Adv. Mater.*, 2010, **22**, 734.

[S8] L. Tang, R. Ji, X. Cao, J. Lin, H. Jiang, X. Li, K. S. Teng, C. M. Luk, S. Zeng, J. Hao and S. P. Lau, *ACS Nano*, 2012, **6**, 5102.

[S9] R. J. Smith, P. J. King, M. Lotya, C. Wirtz, U. Khan, S. De, A. O'Neill, G. S. Duesberg, J. C. Grunlan, G. Moriarty, J. Chen, J. Wang, A. I. Minett, V. Nicolosi and J. N. Coleman, *Adv. Mater.*, 2011, **23**, 3944.